Overlapping Cell Segmentation with Shape Prior

Evan Yi-Wen Wang, Albert Kai-Sun Wong

Department of Electronic and Computer Engineering
Hong Kong University of Science and Technology
Hong Kong
Email: {ywangda, eealbert}@ust.hk

Abstract—**Cell segmentation is a critical task in fully automatic computer cytology diagnosis. Overlapping cells pose a major challenge to cell segmentation because of blurred edges and inhomogeneous cytoplasm. In this paper, we propose a novel energy functional and formulate the boundary identification problem as a problem to minimize this energy functional together with a shape prior. The terms of our energy functional are designed to exploit both the edge and regional features, and the shape prior is derived from low rank optimization. For the non-convex minimization problem, we formulate an efficient monotone Accelerated Proximal Gradient with Linesearch (APGL) algorithm. We evaluate our proposed method using the International Symposium on Biomedical Imaging (ISBI) 2014 and 2015 challenge datasets. Results demonstrate that our method produces competitive accuracy compared to state-of-the-art methods.**

Keywords–Cervical cells; Shape prior; Low-rank optimization.

I. INTRODUCTION

Cervical cancer, which arises from abnormal growth of cervical cells, is the fourth most common cause of women's deaths from cancer. About 70% of these deaths occur in developing countries [1]. Fortunately, the incidence of cervical cancer has been significantly reduced by more than 50% over the past 30 years, mainly due to the widespread cervical cytology screening [2]. Until now, inspection of the cytology image has been done mainly manually, and the inspection process is labor intensive and suffers from inter and intra-observer variability. Hence, fully automatic computer diagnosis has attained great attention.

Cell segmentation is one of the critical steps in computer-aided diagnosis. In this step, individual cells are identified and their nuclei and cytoplasm are detected. The segmentation of overlapping cytoplasm is particularly challenging because of weak edges and inhomogeneous cytoplasm. Numerous attempts have been made to address the problem of overlapping cells. Lu et al. [3] proposed a joint optimization method using multiple level set functions, where different constraints are imposed including contour length, edge strength, cell shape and area of the overlapping regions. However, as pointed out by the authors, the traditional level set method used has issues with the initial segmentation and the re-initialization of the distance function. Hansang Lee et al. [4] proposed an improved algorithm by combining superpixels and cell-wise contour refinement through graph cuts, thus enhancing the oversegmentation method, which suffers from noisy and inaccurate boundaries, especially for overlapping regions. However, their contour refinement has the drawback of sometimes extracting boundaries along nucleus due to the nucleus having

the strongest boundary with large contrast. Phoulady et al. [5] proposed to use multiple images each with a different focal to delineate the cytoplasm corresponding to each nucleus. Since the edge features are not fully exploited for the cytoplasm segmentation, the performance of the algorithm is insufficient. Ushizima et al. [6] proposed a new algorithm for cytoplasm segmentation using a combination of nuclear narrow-band seeding, Voronoi diagram and graph-based region growing. They partition the cell mass into convex polygons such that only one nucleus is located in each Voronoi polygon. However, they assume that all segment lines have equal distances to the nearest nucleus - an assumption that is unrealistic for most overlapping cells. Nosrati et al. [7] proposed a variational approach for segmenting overlapping cells in Pap smear images. They exploit the regional prior, distance prior between a nucleus and its corresponding cytoplasm boundary, elliptical shape prior, and an overlap constraint that induces neighbouring cytoplasm to be excluded from one another. Compared to overlapping cytoplasm detection, nucleus detection is easier. Al-Kofahi et al. [8] proposed to segment cell nucleus using a combination of approaches. In their proposal, nuclear seed points are detected by multiscale Laplacian-of-Gaussian filtering constrained by adaptive scale selection and are used to perform an initial segmentation. A graph cuts algorithm incorporating alpha expansions and graph coloring is used to refine the segmentation. Plissiti et al. [9] used morphological analysis to detect the candidate nucleus centroids and refine the segmentation based on prior knowledge.

An outline of our method is summarized in Figure 1. Our approach consists of four main steps: nucleus localization, mass detection, coarse cytoplasm formation, and fine cytoplasm refinement. In step one, cell nuclei are detected by a Maximally Stable Extremal Regions (MSER) [10] detector and outliers which are tiny areas with low circularity are removed. In step two, the cell masses are extracted through triangle thresholding [11]. In step three, the coarse cytoplasm are generated via Simple Linear Iterative Clustering (SLIC) [12]. The superpixels are clustered based on distance measurement. In the final step, we apply an effective energy functional to refine the coarse cytoplasm. The energy functional consists of four terms: shape prior, regional prior, edge prior and regularized prior. The main contributions of our work are the shape prior construction, energy functional formulation, and the optimization strategy to minimize the energy functional.

In Section II, we give details on the construction of the shape prior using low rank optimization and the formulation of the energy terms that attract the active contour to different types of features. In Section III, we present a novel and effi-

cient algorithm that solves the energy minimization problem. In Section IV, we address the applicability of our method to cervical cell segmentation and present the performance of our method compared to three existing algorithms. Results demonstrate that our method generally shows competitive performance for the ISBI 2014 and 2015 public challenge datasets. Finally, Section V discusses some issues and provides a summary for our work.
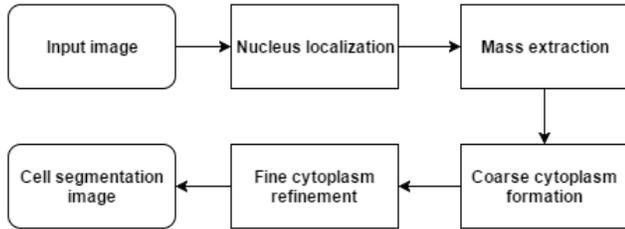
Figure 1. The workflow for overlapping cell segmentation.

II. MODEL SETUP AND PROBLEM FORMULATION

In this section, we show the construction of the shape prior using low rank optimization and the formulation of the energy terms that attract the active contour to different types of features.

A. Shape similarity

To cope with misleading features in images, shape prior is widely used to guide the segmentation process. It has been shown [13] [14] that for a matrix made up of parametric contours of shapes as column vectors, the rank of the matrix can act as a measure of the similarity of the shapes.

We use a vector $\mathbf{c} = [x_1, \ldots, x_n, y_1, \ldots, y_n]^T \in \mathbb{R}^{2n}$ as a parametric contour on the 2D plane, where (x_i, y_i) is a point on the contour. Assume there are k contours $\mathbf{c}_1, \ldots, \mathbf{c}_k$, and $\mathbf{c}_i (i \neq 1)$ is produced by $\mathbf{c}_1$ via affine transformation (i.e., translation, rotation and scaling). Then, the matrix made up of these contours has the following property

$$rank([\mathbf{c}_1, ..., \mathbf{c}_k]) \leq 6 \qquad (1)$$

This property is well-known but a quick proof is given here. $\mathbf{p}'$ and $\mathbf{p}$, the coordinates of a point before and after a shape change through affine transformation, follow the following relation: $\mathbf{p}' = \mathbf{A}\mathbf{p} + \mathbf{T}$. Since $\mathbf{c}_i$ is generated by $\mathbf{c}_1$ through affine transformation, we can express $\mathbf{c}_i$ as $\mathbf{c}_i = \mathbf{C}_1\mathbf{w}$ where

$$\mathbf{C}_1 = \begin{bmatrix} \mathbf{c}_x^1 & \mathbf{0} & \mathbf{c}_y^1 & \mathbf{0} & \mathbf{1} & \mathbf{0} \\ \mathbf{0} & \mathbf{c}_x^1 & \mathbf{0} & \mathbf{c}_y^1 & \mathbf{0} & \mathbf{1} \end{bmatrix},$$

$$\mathbf{w}_i = [a_{11}^i, a_{21}^i, a_{12}^i, a_{22}^i, t_1^i, t_2^i]^T.$$

Here, $\mathbf{c}_x^1 = [x_1, \ldots, x_n]^T$, $\mathbf{c}_y^1 = [y_1, \ldots, y_n]^T$, and a_{jk}^i and t_j^i denote the elements of $\mathbf{A}$ and $\mathbf{T}$. It is straightforward that $[\mathbf{c}_1, ..., \mathbf{c}_k] = \mathbf{C}_1[\mathbf{w}_1, ..., \mathbf{w}_k]$, and $\mathbf{w}_i$ has 6 rows. Therefore, $rank([\mathbf{c}_1, ..., \mathbf{c}_k]) \leq 6$.

Essentially, the rank of the matrix $[\mathbf{c}_1, ..., \mathbf{c}_k]$ represents the degrees of freedom of these shape changes. If we impose a low rank constraint on the matrix, shape changes such as, translation, rotation, and scaling will be allowed.

B. Active contour

In classical active contour models, there are generally two types of energy functional: edge-based [15] and region-based [16]. Next, we briefly review these models.

Let Ω, $\partial\Omega$ denote a bounded open set of $\mathbb{R}^2$ and the boundary of Ω respectively.

The edge-based snake model is to find the contour that produces:

$$\inf_{C(s)} E(C(s)) \qquad (2)$$

where

$$E(C(s)) = \mu \int_0^1 |C'(s)|^2 ds + \nu \int_0^1 |C''(s)| ds$$
$$- \lambda \int_0^1 |\nabla I_0(C(s))|^2 ds$$

is the energy functional.

Here, $C(s) \in \partial\Omega$ denotes a parameterized curve, I_0 denotes a given image, and μ, ν, λ are positive parameters. The first two terms in the energy functional are considered the internal energy, which controls the smoothness of the curve. The last term is considered the external energy, which attracts the curve to stop at the points of maxima $|\nabla I_0|$. Through minimizing $E(C(s))$, we are trying to locate the curve at the boundary of the object while keeping the curve itself as smooth as possible.

The region-based snake model is to find the contour that produces

$$\inf_{C(x,y),v_1,v_2} E(C(x,y), v_1, v_2) \qquad (3)$$

where

$$E(C(x, y), v_1, v_2) = \mu \cdot Length(C(x, y))$$
$$+ \nu \cdot Area(in(C(x, y)))$$
$$+ \lambda_1 \iint_{in(C(x,y))} |I_0(x, y) - v_1|^2 dx dy$$
$$+ \lambda_2 \iint_{out(C(x,y))} |I_0(x, y) - v_2|^2 dx dy$$

Here, $C(x, y) \in \Omega$ is a curve specified by a collection of points (x_i, y_i), I_0 denotes a given image, and v_1, v_2 respectively represent the average intensity of I_0 inside and outside $C(x, y)$. $\mu, \nu, \lambda_1, \lambda_2$ represent positive parameters. The first two terms are regularizing terms, which control the length of curve C and the area inside curve C. The last two terms are fitting terms. The basic idea of this model can be explained by a simple case. Assume the image I_0 is made up of two homogenous regions. The fitting terms are zero if and only if the curve is located at the boundary of the two regions.

C. Energy functional with shape prior

To fully exploit the edge-based and region-based active contour models, we propose to revise the energy functional and include a shape prior such that the problem becomes:

$$\inf_{C(x,y),v_1,v_2} E(C(x,y), v_1, v_2)$$
$$s.t. \quad rank(\Phi_t(C(x, y))) \leq N \qquad (4)$$

where,

$$E(C(x,y)) = \mu \iint_{on(C(x,y))} |\nabla C(x,y)|^2 dxdy$$
$$+ \nu \iint_{on(C(x,y))} |\triangle C(x,y)|^2 dxdy$$
$$+ \lambda_1 \iint_{on(C(x,y))} \frac{1}{1+|\nabla G_\sigma * I_0|^2} dxdy$$
$$+ \lambda_2 \iint_{in(C(x,y))} |I_0 - v_1|^2 dxdy$$
$$+ \lambda_3 \iint_{out(C(x,y))} |I_0 - v_2|^2 dxdy$$

Here, $C(x,y)$ denotes a curve. For simplicity, we replace $C(x,y)$ by C for the rest of the paper. $\mu, \nu, \lambda_1, \lambda_2, \lambda_3$ are determined by validation on the ISBI datasets. v_1, v_2 respectively represent the average intensity of I_0 inside and outside C. To smooth the image, we use a 2-dimensional Gaussian kernel

$$G_\sigma = \frac{1}{\sqrt{2\pi\sigma^2}} e^{\frac{x^2+y^2}{2\sigma^2}}.$$

Let $\Phi_t(C) = [C_{prior}, C_1^*, ...C_t^*, C]$. It contains the shape prior contour and a set of sub-optimal contour candidates and an unknown contour. C_{prior} can be arbitrary shape. Here, C_{prior} is a circular shape contour based on our task, and $C_1^*, ..., C_t^*$ are generated during the low rank minimization according to (5).

In general, the rank minimization problem is NP-hard. Therefore, relaxation is a common way to make the problem tractable. We use nuclear norm, which is proven to be the tightest convex surrogate of rank [17], to approximate the rank function, and relax the origin problem (4) to:

$$\inf_C E(C) + \lambda \|\Phi_t(C)\|_* \tag{5}$$

where $\|\Phi_t(C)\|_*$ denotes the nuclear norm of the matrix $\Phi_t(C)$. Suppose the rank of $\Phi_t(C)$ is r, then $\|\Phi_t\|_* = \sum_{i=1}^r \sigma_i$, where σ_i is the singular value of Φ_t. Hence, the nuclear norm can be viewed as the $l1$-norm of the vector of singular values.

III. THE PROPOSED MINIMIZATION ALGORITHM

Proximal gradient is one of the most popular methods for solving the problem in (5). To illustrate it, we consider a general unconstrained non-smooth non-convex optimization minimization problem:

$$\min_{\mathbf{X}} F(\mathbf{X}) + \lambda G(\mathbf{X}) \tag{6}$$

where F is a differentiable and G is a convex function. Further, F is assumed to be Lipschitz continuous: $\|\nabla F(\mathbf{X}_1) - \nabla F(\mathbf{X}_2)\| < \tau \|\mathbf{X}_1 - \mathbf{X}_2\|$. Therefore, F can be approximated locally as a quadratic function at $\mathbf{X}^k$ such that:

$$Q_\tau(\mathbf{X}, \mathbf{X}^k) = F(\mathbf{X}^k) + \langle \nabla F(\mathbf{X}^k), \mathbf{X} - \mathbf{X}^k \rangle$$
$$+ \frac{\tau}{2} \|\mathbf{X} - \mathbf{X}^k\|_F^2 + \lambda G(\mathbf{X})$$
$$= \frac{\tau}{2} \| \mathbf{X} - [\mathbf{X}^k - \frac{1}{\tau}\nabla F(\mathbf{X}^k)] \|_F^2 + F(\mathbf{X}^k) \tag{7}$$
$$+ \lambda G(\mathbf{X}) - \frac{1}{2\tau} \| \nabla F(\mathbf{X}^k) \|_F^2$$

where τ is a given positive parameter, $\langle \cdot, \cdot \rangle$ denotes the inner product, and $\| \cdot \|_F$ denotes the Frobenius norm. It is straightforward that (7) is a convex function of $\mathbf{X}$, and hence there exists a unique minimizer $\mathbf{X}^*$ such that:

$$\mathbf{X}^* = \arg\min_{\mathbf{X}} Q_\tau(\mathbf{X}, \mathbf{X^k})$$
$$= \arg\min_{\mathbf{X}} \frac{\tau}{2} \| \mathbf{X} - [\mathbf{X^k} - \frac{1}{\tau}\nabla F(\mathbf{X^k})] \|_F^2 \tag{8}$$
$$+ \lambda G(\mathbf{X}) + const$$

Now, we consider a special case of (8),

$$\min_{\mathbf{X}} \frac{\tau}{2} \|\mathbf{X} - \mathbf{S}\|_F^2 + \lambda \|\mathbf{X}\|_* \tag{9}$$

where $G(\mathbf{X}) = \|\mathbf{X}\|_*$. For convenience, we replace $\mathbf{X}^k - \frac{1}{\tau}\nabla F(\mathbf{X}^k)$ with $\mathbf{S} \subset \mathbb{R}^{m \times n}$ and ignore the constant term. Problem (9) has an analytical solution via Singular Value Decomposition (SVD) of $\mathbf{S}$, as has been proved in [18].

$$\mathbf{S} = \mathbf{U\Sigma V}^T, \mathbf{\Sigma} = Diag(\sigma) \tag{10}$$

Here, $\mathbf{U}, \mathbf{V}$ are respectively the left and right eigenvector matrices, and $\mathbf{\Sigma}$ is the diagonal matrix containing the singular values arranged in descending order. Let $\mathbf{x}_+ = max\{\mathbf{x}, \mathbf{0}\}$, and the solution $\mathbf{X}^*$ to (9) is given in closed-form as

$$\mathbf{X}^* = \mathbf{U}Diag((\sigma - \frac{\lambda}{\tau})_+)\mathbf{V}^T \tag{11}$$

In [19], usual Accelerated Proximal Gradient (APG) is extended to the general non-convex case by introducing a monitor variable that satisfies the sufficient descent property. The algorithm consists of the following steps:

$$\mathbf{Y}^k = \mathbf{X}^k + \frac{t^{k-1}}{t^k}(\mathbf{Z}^k - \mathbf{X}^k) + \frac{t^{k-1}-1}{t^k}(\mathbf{X}^k - \mathbf{X}^{k-1}) \tag{12}$$

$$\mathbf{Z}^{k+1} = prox(\mathbf{Y}^k - \tau_y \nabla F(\mathbf{Y}^k)) \tag{13}$$

$$\mathbf{M}^{k+1} = prox(\mathbf{X}^k - \tau_x \nabla F(\mathbf{X}^k)) \tag{14}$$

$$t^{k+1} = \frac{1 + \sqrt{1 + 4(t^k)^2}}{2} \tag{15}$$

$$\mathbf{X}_{k+1} = \begin{cases} \mathbf{Z}_{k+1}, & \text{if } F(\mathbf{Z}_{k+1}) \le F(\mathbf{M}_{k+1}) \\ \mathbf{M}_{k+1}, & \text{otherwise} \end{cases} \tag{16}$$

where τ_x, τ_y are constants satisfying $\tau_x \le \tau$ and $\tau_y \le \tau$. The proximal mapping is defined as $prox(\mathbf{X}) = \arg\min_{\mathbf{U}} G(\mathbf{X}) + \tau \|\mathbf{U} - \mathbf{X}\|^2$. The algorithm is an extension of monotone APG for the convex case. The difference lies in the introduction of the extra $\mathbf{M}$ matrix, which serves as the role of the monitor, and is used in the correction step during the X-update in (16).

To accelerate the convergence of the monotone APG algorithm, we propose to use a linesearch-like technique. In practice, it is desirable to set a smaller value for τ in (11) by performing a linesearch-like technique.

Now, we formally present the monotone accelerated proximal gradient with linesearch (APGL) algorithm, which is outlined as Algorithm 1.

Algorithm 1 Monotone APGL

Require: $\mathbf{X}^1 = \mathbf{X}^0, \mathbf{Z}^1 = \mathbf{Z}^0, t^1 = t^0, \tau^1 = \tau^0,$
$\eta \in (0, 1)$
for $k = 1$ to maximum iterations **do**
$\quad \mathbf{Y}^k = \mathbf{X}^k + \dfrac{t^{k-1}}{t^k}(\mathbf{Z}^k - \mathbf{X}^k) + \dfrac{t^{k-1} - 1}{t^k}(\mathbf{X}^k - \mathbf{X}^{k-1})$
$\quad \widehat{\tau_1} = \eta \tau^{k-1}$
$\quad$ **for** $j = 1$ to maximum iterations **do**
$\qquad \mathbf{Z}^{k+1} = \text{prox}(\mathbf{Y}^k - (\widehat{\tau_j})^{-1}\nabla F(\mathbf{Y}^k))$
$\qquad \mathbf{M}^{k+1} = \text{prox}(\mathbf{X}^k - (\widehat{\tau_j})^{-1}\nabla F(\mathbf{X}^k))$
$\qquad \mathbf{X}^*_{\widehat{\tau_j}} = \begin{cases} \mathbf{Z}_{k+1}, & \text{if } \quad F(\mathbf{Z}_{k+1}) \leq F(\mathbf{M}_{k+1}) \\ \mathbf{M}_{k+1}, & \text{otherwise} \end{cases}$
$\qquad$ **if** $F(\mathbf{X}^*_{\widehat{\tau_j}}) \leq Q_{\widehat{\tau_j}}(\mathbf{X}^*_{\widehat{\tau_j}}, \mathbf{Y}^k)$ **then**
$\qquad\quad \tau^k = \widehat{\tau_j},$ **break**
$\qquad$ **else**
$\qquad\quad \widehat{\tau_{j+1}} = \min\left\{\eta^{-1}\widehat{\tau_j}, \tau^0\right\}$
$\qquad$ **end if**
$\quad$ **end for**
$\quad \mathbf{X}^{k+1} = \mathbf{X}^*_{\tau^k}$
$\quad t^{k+1} = \dfrac{1 + \sqrt{1 + 4(t^k)^2}}{2}$
$\quad$ **if** $\left\|\mathbf{X}^{k+1} - \mathbf{X}^k\right\|^2_F <$ tolerance **then**
$\qquad$ **return**
$\quad$ **end if**
end for

Figure 2. Monotone APGL.

Figure 3. The workflow and methods for overlapping cell segmentation.

IV. EXPERIMENT AND RESULTS

The outline of our cytoplasm segmentation method is summarized in Figure 2 and Figure 3. Now we describe our complete method in six steps: image smoothing, edge detection, mass extraction, nucleus localization, coarse cytoplasm estimation and fine cytoplasm refinement. An example input image is shown in Figure 3(a). First, we apply a bilateral filter to reduce noise and preserve edges. Result is shown in Figure 3(b). Then cell masses are extracted by triangle method [13], and result is shown in Figure 3(c). Edges are detected by SLIC [12], as shown in Figure 3(d). Cell nuclei are segmented by MSER, as shown in Figure 3(e). The coarse cytoplasm is generated by clustering the superpixels near the nucleus based on distance measurement. Finally, the fine cytoplasm is obtained by our proposed method, as shown in Figure 3(f).

We test our method on datasets released by recent ISBI challenges held in 2014 and 2015. The dataset consists of 16 EDF real cervical cytology images and 945 sythetic images. The 810 synthetic images are used for testing in the quantitative evaluation. The 2015 dataset consists of a collection of 17 multi-layer cervical cell volumes, from which 8 will be used for training and 9 for testing. They are realistic images with overlapping cells and poor contrast. We evaluate our method quantitatively by a set of four metrics. Specifically, first, the Dice coefficient(DC) is measured as $DC = \dfrac{2|A \cap B|}{|A| + |B|}$. For individual cytoplasm segmentation, the Dice coefficient is computed over valid cytoplasm segmentation. A valid segmentation is defined as $DC > 0.7$. Second, the false negative rate (FN_o) is calculated as the proportion of segmentation with $DC \leq 0.7$. In addition, for valid segmentation, the true positive rate (TP_p) and false positive rate (FP_p) are also
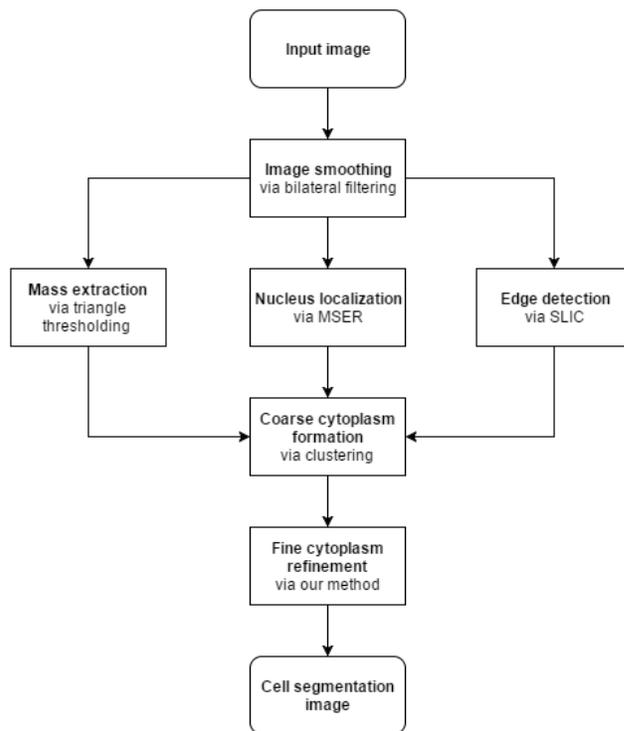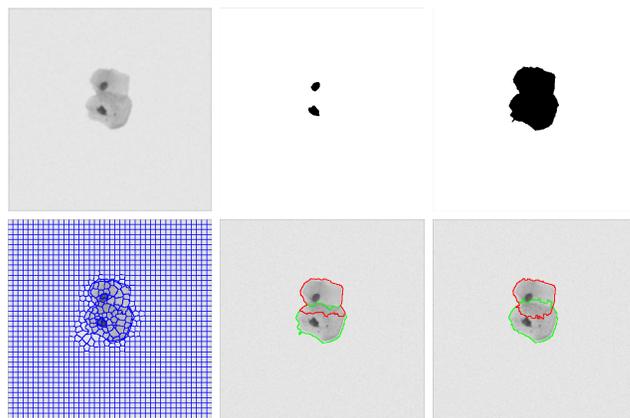
Figure 4. The images of workflow for cytoplasm segmentation. (a) Filtered image (b) Nucleus image (c) Mass image (d) Edge image (e) Coarse cytoplasm image (f) Fine cytoplasm image.

presented as the third and fourth metrics.

We compare our method with existing methods [21]. Specifically, [6], [7] are the winners of ISBI 2014 challenge and [5], [20] are the the winners of ISBI 2015 challenge. In Table I, our proposed method achieves the lowest object-based false negative rate on both datasets. Especially, the object-based false negative rate has been significantly reduced. This means our method generates many more instances of valid segmentation than other existing methods.

Figure 4 displays the segmentation results under different degrees of overlapping cells. As shown in the first row, we divide the overlapping cells into three categories: non-overlapping cells, pair overlapping cells, and multiple overlapping cells. The second row shows the results after the coarse contour formation, and the third row displays the results after
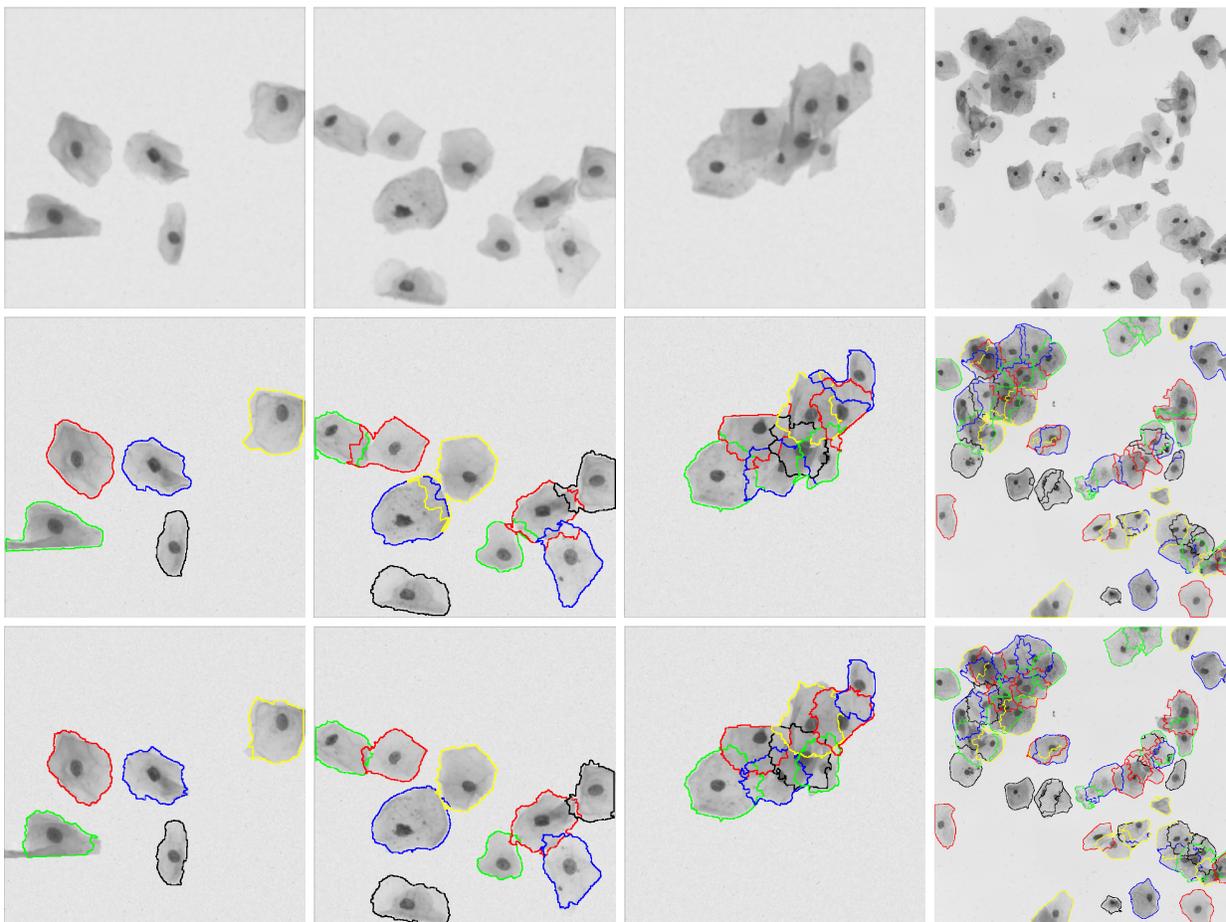
Figure 5. Results of our cytoplasm segmentation results. The top row shows original images. The middle row shows the output after coarse cytoplasm formation. The bottom row shows results of fine cytoplasm refinement.

TABLE I.   EVALUATION AND COMPARISON OF OUR CYTOPLASM SEGMENTATION RESULTS WITH THREE STATE-OF-THE-ART METHODS.

Datasets	Method	FNo	TPp	FPp	DC
ISBI 2014	Ushizima [6]	0.267	0.841	**0.002**	0.872
	Nosrati [7]	0.111	0.875	0.004	0.871
	Lu [3]	0.316	**0.905**	0.004	0.893
	Lee [4]	0.137	0.882	0.002	**0.897**
	Ours	**0.098**	0.901	0.004	0.875
ISBI 2015	Phoulady [5]	0.408	**0.927**	0.003	0.831
	Ramalho [20]	0.501	0.899	0.002	0.856
	Lee [4]	0.434	0.877	**0.001**	**0.879**
	Ours	**0.285**	0.861	**0.001**	0.856

fine cytoplasm refinement. Our method successfully segments all cell cytoplasm in the first two columns with a Dice coefficient around 0.95 for both cases. Our method misses one cytoplasm in the last column due to the severe overlap and weak contrast. The Dice coefficient of the last column is above 0.85, which is still an acceptable result. The segmentation results show a good delineation of the overlapping cytoplasm, and indicate the strong ability of our proposed method in extracting the cell cytoplasm.

In addition, the average running time of our method is about 2.5 seconds for each cell. Our code is written in Matlab and run in Ubuntu. The configuration is a notebook with Intel core i7 and 16 GB RAM.

V. DISCUSSION AND CONCLUSION

In the experimental results, our proposed method in general achieves better performance than the three existing methods. Especially, we observe that the object-based false negative rate has been greatly reduced. We attribute the improvement to the cytoplasm refinement via our proposed method. Since we achieve the highest true positive rate, it is reasonable that our false positive rate is slightly higher than other methods. According to the qualitative results in Figure 4, our approach successfully segments the individual cytoplasm for most cells under different degrees of overlap. Examining the results in Figure 4, we can see that the shape prior plays an important role in fine cytoplasm refinement. The shape prior makes the cytoplasm more elliptical. It is the key factor for improving the false negative rate. But, a point that needs to be addressed

is that, as shown in the first column of Figure 4, the fine cytoplasm refinement actually degrades the result for the cell in green because the shape prior rejects the non-elliptical protrusion on the left-side of the cell.

In conclusion, we have proposed a novel fully automatic segmentation method for overlapping cells. The main contributions of our work are the shape prior construction, energy functional formulation, and the optimization strategy to minimize the energy functional. The shape prior is modeled using low rank optimization to deal with the weak edges and low contrast in overlapping cells. The terms of the energy functional are designed to exploit both the edge and regional features. The monotone APGL algorithm presented solves our non-smooth non-convex problem efficiently. We test our proposed method on the ISBI 2014 and 2015 challenge datasets, and our method shows competitive accuracy compared with existing state-of-the-art methods.

REFERENCES

[1] B. Stewart, C. P. Wild *et al.*, "World cancer report 2014," *World*, 2016.

[2] N. Behtash and N. Mehrdad, "Cervical cancer: screening and prevention," *Asian Pac J Cancer Prev*, vol. 7, no. 4, pp. 683–6, 2006.

[3] Z. Lu, G. Carneiro, and A. P. Bradley, "An improved joint optimization of multiple level set functions for the segmentation of overlapping cervical cells," *IEEE Transactions on Image Processing*, vol. 24, no. 4, pp. 1261–1272, 2015.

[4] H. Lee and J. Kim, "Segmentation of overlapping cervical cells in microscopic images with superpixel partitioning and cell-wise contour refinement," in *Proceedings of the IEEE Conference on Computer Vision and Pattern Recognition Workshops*, 2016, pp. 63–69.

[5] H. A. Phoulady, D. B. Goldgof, L. O. Hall, and P. R. Mouton, "An approach for overlapping cell segmentation in multi-layer cervical cell volumes," *The Second Overlapping Cervical Cytology Image Segmentation Challenge-IEEE ISBI*, 2015.

[6] D. M. Ushizima, A. G. Bianchi, and C. M. Carneiro, "Segmentation of subcellular compartments combining superpixel representation with voronoi diagrams," *Overlapping Cervical Cytology Image Segmentation Challenge-IEEE ISBI*, pp. 1–2, 2014.

[7] M. S. Nosrati and G. Hamarneh, "A variational approach for overlapping cell segmentation," *ISBI Overlapping Cervical Cytology Image Segmentation Challenge*, pp. 1–2, 2014.

[8] Y. Al-Kofahi, W. Lassoued, W. Lee, and B. Roysam, "Improved automatic detection and segmentation of cell nuclei in histopathology images," *IEEE Transactions on Biomedical Engineering*, vol. 57, no. 4, pp. 841–852, 2010.

[9] M. Plissiti, A. Charchanti, O. Krikoni, and D. Fotiadis, "Automated segmentation of cell nuclei in pap smear images," in *Proc. IEEE International Special Topic Conference on Information Technology in Biomedicine*. Citeseer, 2006, pp. 26–28.

[10] J. Matas, O. Chum, M. Urban, and T. Pajdla, "Robust wide-baseline stereo from maximally stable extremal regions," *Image and vision computing*, vol. 22, no. 10, pp. 761–767, 2004.

[11] G. Zack, W. Rogers, and S. Latt, "Automatic measurement of sister chromatid exchange frequency." *Journal of Histochemistry & Cytochemistry*, vol. 25, no. 7, pp. 741–753, 1977.

[12] R. Achanta, A. Shaji, K. Smith, A. Lucchi, P. Fua, and S. Süsstrunk, "Slic superpixels compared to state-of-the-art superpixel methods," *IEEE transactions on pattern analysis and machine intelligence*, vol. 34, no. 11, pp. 2274–2282, 2012.

[13] X. Zhou, X. Huang, J. S. Duncan, and W. Yu, "Active contours with group similarity," in *Proceedings of the IEEE Conference on Computer Vision and Pattern Recognition*, 2013, pp. 2969–2976.

[14] X. Zhou, C. Yang, H. Zhao, and W. Yu, "Low-rank modeling and its applications in image analysis," *ACM Computing Surveys (CSUR)*, vol. 47, no. 2, p. 36, 2015.

[15] M. Kass, A. Witkin, and D. Terzopoulos, "Snakes: Active contour models," *International journal of computer vision*, vol. 1, no. 4, pp. 321–331, 1988.

[16] T. F. Chan and L. A. Vese, "Active contours without edges," *IEEE Transactions on image processing*, vol. 10, no. 2, pp. 266–277, 2001.

[17] M. Fazel, "Matrix rank minimization with applications," Ph.D. dissertation, PhD thesis, Stanford University, 2002.

[18] J.-F. Cai, E. J. Candès, and Z. Shen, "A singular value thresholding algorithm for matrix completion," *SIAM Journal on Optimization*, vol. 20, no. 4, pp. 1956–1982, 2010.

[19] H. Li and Z. Lin, "Accelerated proximal gradient methods for non-convex programming," in *Advances in Neural Information Processing Systems*, 2015, pp. 379–387.

[20] G. L. Ramalho, D. S. Ferreira, A. G. Bianchi, C. M. Carneiro, F. N. Medeiros, and D. M. Ushizima, "Cell reconstruction under voronoi and enclosing ellipses from 3d microscopy," in *IEEE International Symposium on Biomedical Imaging (ISBI)*, 2015.

[21] Z. Lu, G. Carneiro, A. Bradley, D. Ushizima, M. S. Nosrati, A. Bianchi, C. Carneiro, and G. Hamarneh, "Evaluation of three algorithms for the segmentation of overlapping cervical cells," *IEEE journal of biomedical and health informatics*, 2016.